

First principles calculations of lattice thermal conductivity in mono- and bi-layer graphene

B. D. Kong,¹ S. Paul,² M. Buongiorno Nardelli,^{2,3,*} and K. W. Kim^{1,†}

¹*Department of Electrical and Computer Engineering,
North Carolina State University, Raleigh, NC 27695-7911*

²*Department of Physics, North Carolina State University, Raleigh, NC 27695-8202*

³*Computer Science and Mathematics Division,
Oak Ridge National Laboratory, Oak Ridge, TN 37831*

Abstract

Using calculations from first principles we have investigated the lattice thermal conductivity of ideal mono- and bi-layer graphene sheets. Our results demonstrate that the intrinsic thermal conductivity of both mono- and bi-layer graphene is around $2200 \text{ Wm}^{-1}\text{K}^{-1}$ at 300 K, a value close to the one observed theoretically and experimentally in graphite basal plane, and at higher temperatures it decreases with the expected T^{-1} dependence. The little variation between mono- and bi-layer thermal conductivity suggests that increasing the number of layers does not affect significantly the in-plane thermal properties of these systems.

Although carbon-based low dimensional materials have been subject of intense investigations for decades, the recent synthesis of graphene, a single 2-dimensional sheet of hexagonal carbon in the honeycomb lattice, has opened new avenues of research in the search of novel, alternative materials for microelectronics.¹ The peculiar electronic structure of graphene¹ implies that electrons have a negligible effective mass around the K point of the Brillouin zone (Dirac point) and thus a high electrical conductivity. However, electric currents are inherently coupled with Joule heating so it is imperative to investigate the thermal property of these systems to insure proper operations of an eventual device. Usually a good electric conductor is a good thermal conductor. However, this expectation is broken in the case of diamond, another kind of carbon-base crystal, which exhibit a high thermal conductivity regardless of its large band gap and low electric conductivity. Graphite, the closest relative of graphene in the family of carbon-based materials, displays high thermal conductivity along the basal plane and, not surprisingly, two orders of magnitude smaller thermal conductivity along the c -crystallographic axis.²

There is a relatively large scattering in the experimental data for the thermal conductivity of highly oriented graphite and graphene systems. Ref. 2 reports values of thermal conductivity in the range $1660 - 1880 \text{ Wm}^{-1}\text{K}^{-1}$. Balandin *et al.*³ measured values around $4840 - 5300 \text{ Wm}^{-1}\text{K}^{-1}$ for a suspended graphene mono-layer. More recently, Nika *et al.*⁴ reported their theoretical investigation on the thermal conductivity of mono-layer graphene and publish values in a range between $3000 - 6500 \text{ Wm}^{-1}\text{K}^{-1}$, depending on the choice of Grüneisen parameters, γ , which had values ranging from 0.8 to 2.0 as deduced from Ref 12. This particular study was based on the use of a valence force field method which resolves all interatomic forces into bond-stretching and bond bending modes.^{4,5} and the Grüneisen parameters were assumed to be constant for each phonon branch.⁴ Comparable values of thermal conductivity have also been observed in Carbon Nanotubes (CNT): Kim *et al.*⁶ reported approximately $3000 \text{ Wm}^{-1}\text{K}^{-1}$ as a thermal conductivity of a multi-wall CNT with 140 \AA diameter. Pop *et al.*⁷ observed $2800 - 3900 \text{ Wm}^{-1}\text{K}^{-1}$ for single-wall CNT with diameters between $0.5 - 10 \mu\text{m}$ at room temperature. Both experiments were performed on a single suspended nanotube by heating it with electrical current.

In order to resolve this apparent spread in the values of thermal conductivity and understand the interplay between the number of layers and the thermal response of these systems we have investigated the intrinsic lattice thermal conductivity of ideal mono- and bi- layer

graphene using phonon dispersion relations and lattice anharmonicity parameters calculated from first principles methods. Our results show that mono- and bi-layer graphene sheets have an intrinsic thermal conductivity superior to usual bulk solids except diamond which has $600 \sim 2000 \text{ Wm}^{-1}\text{K}^{-1}$ ⁸.

The lattice thermal conductivity κ of a crystal at finite temperature T can be written as

$$\kappa = \sum_{\lambda} \kappa_{\lambda} \quad (1)$$

$$\kappa_{\lambda} = \sum_{\mathbf{q}} (\mathbf{v}(\mathbf{q}) \cdot \mathbf{t})^2 \tau(\mathbf{q}) C_{ph}(\omega) \quad (2)$$

where \mathbf{t} is a unit vector in the direction of the thermal gradient ∇T , $\mathbf{v}(\mathbf{q})$ is the group velocity of the phonon modes, and $\tau(\mathbf{q})$ is their life time.^{9,10,11} Here, the index λ runs over the phonon modes and $C_{ph}(\omega)$ is the contribution of phonon modes to the specific heat whose form is

$$C_{ph}(\omega) = \hbar\omega \frac{dN^0}{dT} = \frac{(\hbar\omega)^2}{k_B T^2} \frac{\exp(\hbar\omega/k_B T)}{[\exp(\hbar\omega/k_B T) - 1]^2} \quad (3)$$

where k_B is Boltzmann constant and \hbar is Plank constant. In order to evaluate accurately the lattice thermal conductivity one needs to obtain the phonon group velocity $\mathbf{v}(\mathbf{q})$ from realistic phonon dispersion relations and to estimate the phonon life time from a careful consideration of the possible relaxation mechanisms.

As shown very elegantly in Ref 2, one can calculate the graphite thermal conductivity along the basal plane considering only the LA and TA branches. The assumption is that the phonon dispersion of graphite has cylindrical shape and the ZA modes strongly interact only along the c -direction, mainly due to the large spacing and the weak bonding between the layers. Since the group velocities of the optical modes are considerably smaller than those of the acoustic modes, optical branches can be disregarded. Therefore, we can consider only TA and LA modes in the range above the temperature which corresponds to the highest ZA frequency and we can replace the first Brillouin zone (FBZ) with a circular cylinder and define the average sound velocity $\langle v \rangle$ for the two-dimensional phonon gas consisting of LA and TA modes as: $2/\langle v \rangle^2 = 1/\langle v_{LA} \rangle^2 + 1/\langle v_{TA} \rangle^2$. Recent first principles calculations of phonon dispersion in graphite^{12,13} and our own results validate this approach since the phonon dispersion curves along the $\Gamma - A$ axis are almost flat, implying that the FBZ of graphite looks like a circular column. Graphene sheets inherently have a two dimensional nature so it seems reasonable to accept these assumptions for the high temperature range in

which the role of ZA modes is not significant. According to our calculations, the maximum of ZA mode is at 535 cm^{-1} . This frequency corresponds to 123 K ($k_B T = \hbar \omega$), validating our assumption for any T larger than that.

We evaluated the average phonon life time as limited by the anharmonicity of lattice vibrations since this is the most fundamental limiting factor which is not relying on the purity of crystal or boundary termination technology. The analytical expression for the relaxation rate from the anharmonic three-phonon processes are readily derived as:

$$\frac{1}{\tau_\lambda} = 2\gamma_\lambda^2 \frac{k_B T}{M v^2} \frac{\omega^2}{\omega_m} \quad (4)$$

where γ_λ are Grüneisen parameters, k_B is Boltzmann constant, T is temperature, M is the mass of atoms and λ runs over the phonon modes.^{2,9,14} ω_m and v are Debye frequency and the average sound velocity.

The phonon dispersion relations used in this study have been obtained from first principles calculations within Density Functional Theory and Density Functional Perturbation Theory. The predictive power of this approach has been demonstrated by the excellent agreement between theoretical predictions and experimental observations in recent studies on the lattice vibrational modes of graphite and graphene.^{12,13} In this study, the calculation for phonon dispersion and Grüneisen parameters for the mode anharmonicity were obtained by using the PWSCF package of the QUANTUM-ESPRESSO distribution.¹⁵

Fig. shows the calculated phonon dispersions along the high symmetry lines. The phonon frequency values of high symmetry points such as Γ , M, and K can be compared with previous studies and the results for mono-layer graphene are summarized in Table I. The results for bi-layer graphene show a very similar behavior. As shown in the figure, another optical vibrational mode appears at Γ of bi-layer graphene phonon dispersion. This ZO' mode at 78 cm^{-1} is produced by the displacement of the carbon atoms in opposite directions along the c crystalline axis (optical mode). In graphite the same mode has a frequency of 95 cm^{-1} .¹⁶ The agreement of our data with the previous theoretical and experimental studies is clearly excellent. From these accurate phonon dispersion curves we calculated the group velocity $\mathbf{v}(\mathbf{q})$ and the Grüneisen parameter γ_λ for each phonon mode λ . The latter are defined as the negative logarithmic derivative of the frequency of the mode with respect to volume: $\gamma_\lambda = -[a/2\omega_\lambda(\mathbf{q})][d\omega_\lambda(\mathbf{q})/da]$ ^{12,19} where a is the lattice constant. By calculating phonon dispersion relation with small deviation from the original lattice constant and using

the above definition, we computed the Grüneisen parameters over the FBZ as shown in Fig. . In mono-layer graphene, the ZO and ZA modes have negative γ_λ , between -1.38 and -0.17 for ZO, and between -53 and -1.46, for ZA. For the other modes, the values show variations between 0.16 and 2.76. Positive values of γ correspond to a decrease of the frequency of the modes as the lattice parameter increases: the atoms are less tightly bound to their equilibrium position. Inversely, negative values of γ correspond to an increase of the frequencies upon the expansion of the lattice. Since ZA and ZO are out-of-plane transverse polarization modes, one can imagine that if a graphene sheet is expanded, the force to move the atoms in the vertical direction will increase. As for the bi-layer, the dispersion relations for the Grüneisen parameters display an additional contribution corresponding to the ZO' mode. In addition, γ_{ZA} and $\gamma_{ZO'}$ of the bi-layer show slightly different behavior at the Γ point: they are positive. Small values of \mathbf{q} (around Γ) correspond to long wavelength phonons and a positive value of γ means that the atoms are less tightly bound. The variation of γ from negative to positive tells us that the properties of the ZA or ZO' modes' collective movement are different for long wavelength and short wave length: as the volume is increased, and with it the intra-layer distance, $\omega_{ZA,ZO'}$ decreases at Γ . Atoms in both layers loose some of their coherence in the long wavelength vibrational modes. There are two TA and LA modes so the mean value of γ_{TA1} , γ_{TA2} , γ_{LA1} , and γ_{LA2} in the FBZ was found to be 0.52, 0.53, 1.58, and 1.56, respectively.

The normalized thermal conductivity κ/τ is reported in Fig. . The curves are obtained from the *ab initio* phonon dispersion relations and the two-dimensional phonon gas model for infinite mono- and bi-layer graphene sheets along (100) direction from 200 K to 500 K. For mono- and bi- layer, we observe a similar behavior over the calculated temperature range: both show almost the same normalized thermal conductivities. For instance, at $T=300$ K, $\kappa/\tau = 4.78 \times 10^{13} Wm^{-1}s^{-1}$ for mono-layer and $\kappa/\tau = 4.83 \times 10^{13} Wm^{-1}s^{-1}$. In both cases the contribution from the LA mode is larger than the one from the TA mode due to the large group velocity of the LA mode. From the data in Fig. (b), it is evident that the magnitude of the TA and LA modes is decreased when another layer is added to the system; however, also the number of modes doubles so that the normalized conductivity is the same. Moreover, going from mono- to bi-layer graphene, the slope of the TA and LA branches do not change significantly. However, the thickness of the layer doubles, so the contribution from each branch becomes one half of the value of the mono-layer.²¹

The lattice thermal conductivity with phonon mean life time limited by lattice anharmonicity effects is presented in Fig. for the same temperature range of Fig and along the (100) direction. Both mono- and bi- layer graphene display a similar $\sim 1/T$ dependence at high temperature. The values of κ at room temperature (300 K) differ only by $8 \text{ Wm}^{-1}\text{K}^{-1}$. As previously mentioned, the contribution from the LA branch is larger than that from the TA branch in the case of normalized thermal conductivity. However, as shown in the graphs, the TA mode transfers a larger portion of thermal energy than the LA mode in the real thermal conductivity. This is due to the longer phonon life time of TA which is expected from the comparison of the Grüneisen parameters. The LA mode has three times larger γ . Overall, nine times longer phonon mean life time is expected for TA so that this longer life time compensate the smaller group velocity. Klemens *et al.*² predicted $1900 \text{ Wm}^{-1}\text{K}^{-1}$ as the lattice thermal conductivity along the basal plane for the bulk graphite at 300 K. Our results substantially agree with this previous estimate. The small difference, around $300 \text{ Wm}^{-1}\text{K}^{-1}$ at room temperature, that we find can be explained by two reasons. First, in Ref. 2 they assumed $\gamma=2$ for both modes, a choice that eventually decreases the thermal conductivity. Second, they assumed an average sound velocity in the FBZ which could increase the thermal conductivity since the actual group velocity of phonon modes decreases when \mathbf{q} approaches the zone boundary. The Debye frequencies ω_m of two dimensional phonon gas in mono- and bi- layer graphene are 1265 cm^{-1} and 1243 cm^{-1} respectively and those almost correspond to the maximum frequencies of the LA mode at the zone boundary which supports the assumption that the frequency below ω_m (TA and LA) contributes to the thermal conduction. Finally, in Fig. we present the angular dependence of the thermal conduction. θ in the figure is the angle between the direction of the thermal gradient and the (110) crystalline direction. The angular dependence was calculated for different thermal gradient directions where, however, we observe only a negligible variation (less than 0.1% at 300 K).

When it comes to realistic finite graphene nanoribbon, other possible scattering mechanisms can arise, in particular scattering by impurities and by the discontinuous structure of the ribbon side terminations. To evaluate these effects one should both measure the density of substitutional impurity atoms and the mass difference between the impurity atoms and the carbon atoms and gain a more complete understanding of the geometry of the system. Both pieces of information are not yet readily available from the current status of research on these systems. Therefore, our values for the intrinsic lattice thermal conductivity of

mono- and bi- layer graphene can be regarded as a theoretical upper limit of the thermal conductivity of more realistic graphene nanoribbons.

This work was supported, in part, by the NERC/NIST SWAN-NRI research center and the DARPA/HRL CERA program. MBN wishes to acknowledge partial support from the Office of Basic Energy Sciences, U.S. Department of Energy at Oak Ridge National Laboratory under contract DE-AC05-00OR22725 with UT-Battelle, LLC. Calculations have been carried out at the Center for Computational Sciences at ORNL and the NC State University HPC and Grid Computing initiative.

-
- * Electronic address: mbnardelli@ncsu.edu
- † Electronic address: kwk@ncsu.edu
- ¹ A. K. Geim and K. S. Novoselov, *Nat. Mater.* **6**, 183 (2007).
- ² P. G. Klemens and D. F. Pedraza, *Carbon* **32**, 735 (1994).
- ³ A. A. Balandin, S. Chosh, W. Bao, Irene Calizo, D. Teweldebrhan, F. Miao, and C. N. Lau, *Nano Lett.*,**8**, 902 (2008)
- ⁴ D. L. Nika, E. P. Pokatilov, A. S. Askerov, and A. A. Balandin, arXiv:0812.0518v1 (unpublished).
- ⁵ R. M. Martin, *Phys. Rev. B* **1**, 4005 (1974)
- ⁶ P. Kim, L. Shi, A. Majumdar, and P. L. McEuen, *Phys. Rev. Lett.* **87**, 215502 (2001)
- ⁷ E. Pop, D. Mann, Q. Wang, K. Goodson, and H. Dai, *Nano Lett.* **6**, 96 (2006).
- ⁸ R. Berman, P. R. W. Hudson, and M. Martinez, *J. Phys. C.* **6**, L430 (1975).
- ⁹ P. G. Klemens, in *Thermal Conductivity*, edited by R. P. Tye (Academic, London, 1969), Vol. 1, p. 1.
- ¹⁰ J. M. Ziman, *Electrons and Phonons*(Oxford University Press, Oxford, 1960), p. 306.
- ¹¹ A. A. Kiselev, K. W. Kim, and M. A. Stroscio, *Phys. Rev. B* **62**, 6896 (2000).
- ¹² N. Mounet and N. Marzari, *Phys. Rev. B* **71**, 205214 (2005).
- ¹³ N. Bonini, M. Lazzeri, N. Marzari, and F. Mauri, *Phys. Rev. Lett.* **99**, 176802 (2007).
- ¹⁴ P. G. Klemens, in *Solid State Physics*, edited by F. Seitz and D. Turnbull (Academic, New York, 1958), Vol. 7, p. 1.
- ¹⁵ QUANTUM-ESPRESSO is a community project for high-quality quantum-simulation software, based on density-functional theory, and coordinated by Paolo Giannozzi. See <http://www.quantum-espresso.org> and <http://www.pwscf.org>.
- ¹⁶ C. Oshima, T. Aizawa, R. Souda, Y. Ishizawa, and Y. Sumiyoshi, *Solid State Commun.* **65**, 1601 (1988).
- ¹⁷ J. Maultzsch, S. Reich, C. Thomsen, H. Requardt, and P. Ordejón, *Phys. Rev. Lett.* **92**, 075501 (2004).
- ¹⁸ H. Yanagisawa, T. Tanaka, Y. Ishida, M. Matsue, E. Rokuta, S. Otani, and C. Oshima, *Surf. Interface Anal.* **37**, 133 (2005).

- ¹⁹ N. W. Ashcroft and N. D. Mermin, *Solid State Physics* (Holt, Rinehart and Winston, New York, 1976), Chaps. 1 and 25.
- ²⁰ We used the pseudopotentials C.pbe.rrkjus.UPF from the <http://www.quantum-espresso.org> distribution, and a plane wave expansion up to 55 **Ry**. $32 \times 32 \times 1$ Monkhorst-Pack meshes were used with a 0.02 **Ry** Fermi-Dirac smearing in the electronic occupations. We used the theoretical lattice parameter $a = 2.46 \text{ \AA}$ that is in excellent agreement with the experimental value at 300K. The same simulation parameters were used for both mono- and bi-layer graphene setting the intralayer distance to the theoretical minimum 3.36 \AA . The bi-layer graphene geometry is rhombohedral.
- ²¹ We assumed a layer thickness $h = 3.5 \text{ \AA}$ for mono-layer²² and $h = 3.5 + 3.36 = 6.86 \text{ \AA}$ for the bi-layer.
- ²² A. Gupta, G. Chen, P. Joshi, S. Tadigadapa, P. C. Eklund, *Nano Lett.* **6**, 2667 (2006).

Figure Captions

Figure 1(a,b). (Color online) Phonon dispersion of (a) a mono-layer and (b) a bi-layer graphene sheet along the high symmetry line.

Figure 2(a,b,c). (Color online) Grüneisen parameter of (a) a mono-layer and (b) a bi-layer graphene sheets along the high symmetry lines. (c) Two dimensional surface of Grüneisen parameter of a mono-layer graphene sheet over the entire FBZ.

Figure 3.(a,b) (Color online) Normalized thermal conductivity in (100) direction of (a) a mono-layer and (b) a bi-layer graphene sheet.

Figure 4.(a,b) (Color online) Thermal conductivity in (100) direction of (a) a mono-layer and (b) a bi-layer graphene sheet. Inset of (a): the angular dependence of the thermal conductivity of a mono-layer graphene sheet at $T = 300$ K. θ is the angle between the thermal gradient and the (110) direction.

TABLE I: Comparison of the phonon frequencies of graphene at Γ , M, and, K in cm^{-1} from various studies.

	Γ_{ZO}	$\Gamma_{\text{LO/TO}}$	M_{ZA}	M_{TA}	M_{ZO}	M_{LA}	M_{LO}	M_{TO}	K_{ZA}	K_{ZO}	K_{TA}	K_{LA}	K_{LO}	K_{TO}
This study ²⁰	884	1560	473	627	641	1318	1360	1396	532	550	997	1210	1228	1327
Theoretical ^a	881	1554	471	626	635	1328	1340	1390	535	535	997	1213	1213	1288
Experimental	861 ^b	1590 ^b	465 ^b	630 ^b	670 ^b	1290 ^c	1321 ^c	1389 ^d	482 ^d	588 ^d		1184 ^d	1184 ^d	1313 ^c

^aReference 12. Graphene sheets

^bReference 16. Graphite

^cReference 17. Graphene sheets

^dReference 18. Graphite

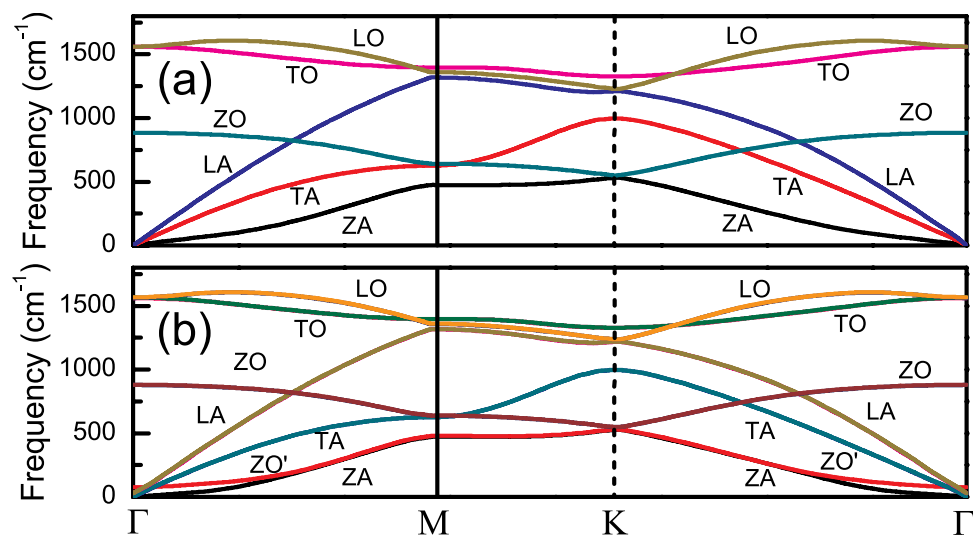


Fig. 1(a,b): Kong *et al.*

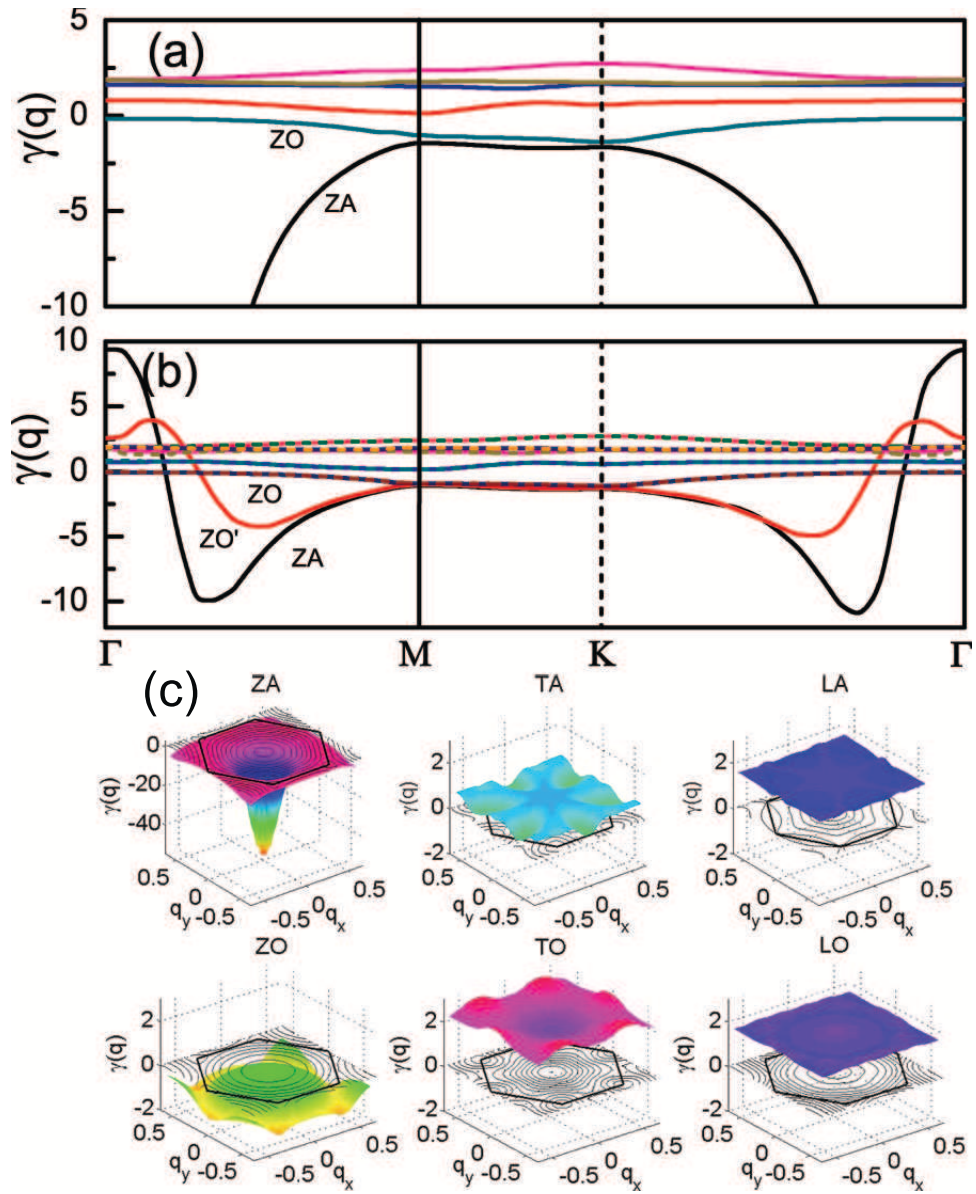


Fig. 2(a,b,c): Kong *et al.*

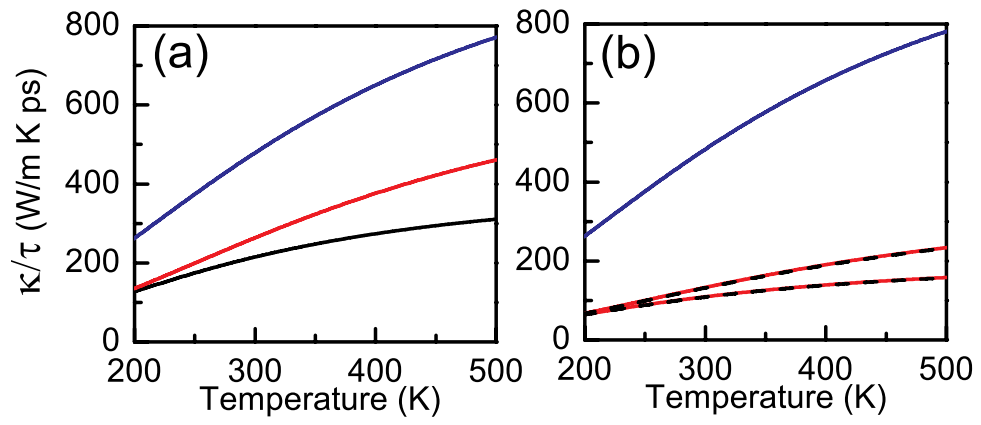


Fig. 3(a,b): Kong *et al.*

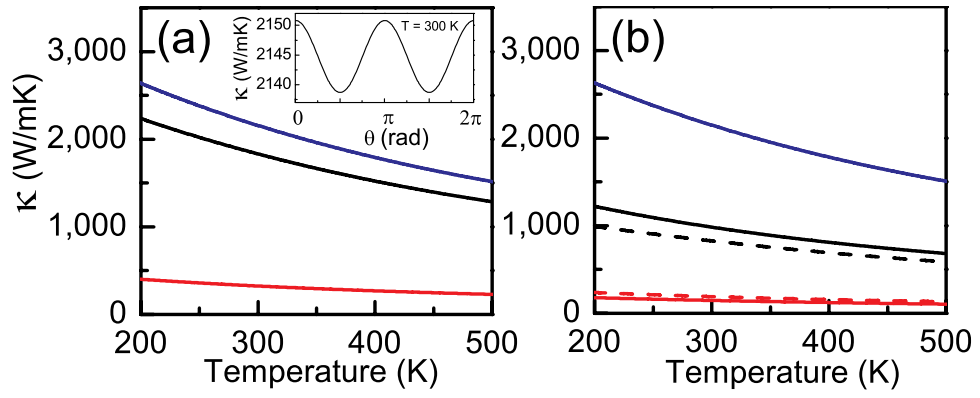


Fig. 4(a,b): Kong *et al.*